Numerical Study of the Effects of Confinement on Concurrent-Flow Flame Spread in Microgravity

Yanjun Li
Department of Mechanical and Aerospace Engineering,
Case Western Reserve University,
10900 Euclid Avenue,
Cleveland, OH 44106
e-mail: yxl1453@case.edu

Ya-Ting T. Liao[1]
Mem. ASME
Department of Mechanical and Aerospace Engineering,
Case Western Reserve University,
10900 Euclid Avenue,
Cleveland, OH 44106
e-mail: yating.liao@case.edu

Paul Ferkul
NASA Glenn Research Center,
21000 Brookpark Road,
Cleveland, OH 44135
e-mail: paul.ferkul@nasa.gov

The objective of this work is to investigate the aerodynamics and thermal interactions between a spreading flame and the surrounding walls as well as their effects on fire behaviors. A three-dimensional transient computational fluid dynamics (CFD) combustion model is used to simulate concurrent-flow flame spread over a thin solid sample in a narrow flow duct. The height of the flow duct is the main parameter. The numerical results predict a quenching height for the flow duct below which the flame fails to spread. For duct heights sufficiently larger than the quenching height, the flame reaches a steady spreading state before the sample is fully consumed. The flame spread rate and the pyrolysis length at steady-state first increase and then decrease when the flow duct height decreases. The detailed gas and solid profiles show that flow confinement has multiple effects on the flame spread process. On one hand, it accelerates flow during thermal expansion from combustion, intensifying the flame. On the other hand, increasing flow confinement reduces the oxygen supply to the flame and increases conductive heat loss to the walls, both of which weaken the flame. These competing effects result in the aforementioned nonmonotonic trend of flame spread rate as duct height varies. Near the quenching duct height, the transient model reveals that the flame exhibits oscillation in length, flame temperature, and flame structure. This phenomenon is suspected to be due to thermodiffusive instability. [DOI: 10.1115/1.4047645]

1 Introduction

Fires in confined spaces (e.g., cavity walls in buildings, transportation vehicles, tunnels) are a major safety concern. They result in significant numbers of injuries, deaths, and property losses every year [1]. In confined spaces, fire behaviors can be very different from fires in open spaces. To address this concern, many past studies have focused on the mechanical (or aerodynamic) interactions between fires and different structures (e.g., corners [2,3], adjacent walls [3], or parallel panels [4]). Other studies have focused on tunnel fires with ventilated flows [5,6]. In most of these studies, fires are simulated experimentally using stationary burners—the flame does not move. However, in most situations, real fires in confined spaces involve flames that themselves move or spread across the fuel.

Flame spread is one of the most important characteristics of a fire, as it determines the available time to control the fire or to escape the area. There have been extensive efforts studying flame spread over solid materials using microgravity experiments. In microgravity, buoyancy is essentially eliminated and hence forced flow can be imposed on the sample independent of other parameters. For concurrent-flow flame spread in microgravity, limiting flame lengths and steady spread rates were predicted by numerical models [7,8]. They were also verified in space experiments for both thick [9] and thin [10,11] samples in low-speed flows using a small flow duct (duct height ~10 cm) aboard the International Space Station (ISS).

In a recent NASA project, a series of large-scale flame spread experiments were conducted in unmanned space vehicles [12,13]. The dimensions of the sample and the flow duct used in these experiments were significantly larger (duct height ~ 40 cm) than prior experiments. Results yielded significantly smaller flame spread rates than seen in previous smaller-scale experiments for the same thin fabric, even when all other environmental conditions (oxygen, pressure, and flow speed) were the same. This observation that flames spread faster in smaller ducts is suspected to be due to thermal expansion during combustion which causes acceleration because the flow is more confined. This is referred to as the chimney effect. The increased radiation heat feedback from duct walls to the flame and to the fuel surface may also be a factor.

Several research groups have conducted numerical studies that address this situation [14–16] For instance, Shih and T'ien studied concurrent-flow flame spread over thin solids in a flow tunnel, using a two-dimensional steady model (capable of only finding steady-state solutions) [14]. Their results showed that the flame spread rate increases when the tunnel height decreases, consistent with the experimentally observed phenomena. However, when the tunnel height is very small, conductive heat loss to the tunnel walls increases, slowing the spread rate. This eventually leads to flame quenching. In their work, Shih and T'ien also documented that no steady-state solution was achieved for some confined conditions (e.g., small duct height, high wall reflectivity). It is suspected that the flame continuously grows while traveling downstream (a transient process) and hence cannot be captured by a steady model.

A similar process was observed independently by Shih [15] and Malhotra et al. [16], who also used steady-state models. In their works, concurrent [15] and opposed [16] flow flame spreads over parallel thin solid fuel sheets in microgravity environments were simulated (using steady two-dimensional models). The fuel sheets were oriented parallel to the flow direction. The flow confined between adjacent sheets is similar to flow in a tunnel (the symmetry planes between the parallel fuel sheets are equivalent to slip adiabatic walls with perfect radiative reflectivity). At first, as the fuel sheets are brought together, the spread rate increases as the separation distance decreases. For intermediate fuel-sheet-separation distances, no steady solutions were obtained unless there was no radiation interaction between the flame and the fuel (radiation was artificially suppressed in the model). When the separation distance is further decreased, the flame spread rate

---

decreases and eventually the flame quenches due to flow resistance, limited thermal expansion, and oxygen starvation.

In this work, we conduct three-dimensional transient numerical simulations on concurrent-flow flame spread over solids in different confined conditions. Flow profiles and thermal interactions between the flame and the surrounding walls are studied in detail, and their effects on flame spread rates are characterized. Last, the three-dimensional transient flame behaviors leading to quenching at highly confined conditions are explored.

2 Numerical Model

The model configuration is shown in Fig. 1. A 30 cm-long, 2.2 cm-wide cotton-blend fabric (75% cotton, 25% fiber-glass) is mounted by a stainless steel sample holder at the center of the flow duct. Two different sample holders are considered in this work (Fig. 1(b)). One sample holder has the same width (7.6 cm) as the flow duct. Another sample holder is narrower than the flow duct, leaving 2 cm gaps between the edges of the sample holder and the duct side walls (see Fig. 1(a)).

The width and length of the flow duct are 7.6 cm and 40 cm, respectively. The height of the flow duct (h) is the parameter in this study. It varies between 0.5 and 9.0 cm. Air flow at 10 cm/s is imposed at the duct inlet. Ignition is achieved by applying an external heat flux with a Gaussian distribution near the upstream leading edge of the sample. The maximum heat flux is

(a)

L = 40 cm

h

gap

igniter

Air flow
10 cm/s

W = 7.6 cm

(b)
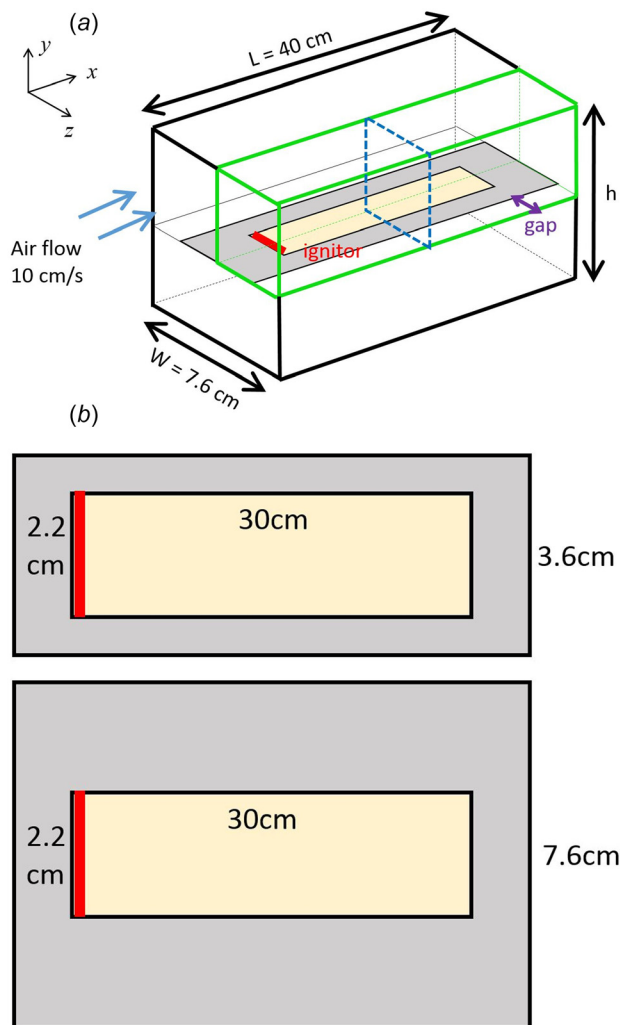
2.2 cm

30cm

3.6cm

2.2 cm

30cm

7.6cm

Fig. 1 Model configuration (a) sample, sample holder, and the flow duct. (b) Both sample setups, narrow and wide sample holders. The plots are not to scale.

2.39 W/cm^2 (occurring at 0.3 cm away from the leading edge) and 98% of the ignition energy is distributed within 0.6 cm from the leading edge. After ignition, the external heat flux is gradually turned off over 3 s in a linear manner. The ambient conditions are at zero gravity with air temperature of 300 K and pressure of 1 atm.

Black surface (emissivity equals to 1) and constant temperature at 300 K are assumed on all duct walls. Symmetry is assumed on the plane along the centerline of the fuel sample and on the plane of the sample half-thickness. This reduces the computational domain to a quarter of the flow duct (marked by the green box in Fig. 1(a)).

Note that this model configuration and sample material are based on previous microgravity experiments aboard the ISS [10,11]. The model has been shown robust and able to capture the transient process of the burning event in the experiments [10]. Also note that in these experiments, flames were observed on both sides on the sample. This justifies the aforementioned symmetry boundary condition imposed on the plane of the sample half-thickness.

In the simulation, in addition to changing the height of the flow duct, we extend the length of the sample and the length of the flow duct from the lengths used in the experiments. This allows additional time for flame development and facilitates observation of the fate of the flame (continuously growing, steady flame spread, or extinction) in different confined conditions.

The numerical model used in this work is based on a previously developed three-dimensional transient computational fluid dynamics (CFD) model. Detailed information, mathematical formulation, and property values can be found in previous papers [10,17–20]. A brief summary of the model is as follows.

The model consists of a gas phase and a solid phase. The gas phase model simulates the combustion and transport processes of the burning event, using direct numerical simulation. It solves three-dimensional transient full Navier–Strokes equations for the conservation of mass, species, momentum, and energy. One-step, second-order, finite rate global Arrhenius kinetics is assumed for the gas-phase reaction. Gas radiation is included by solving the radiation transfer equation. Nonscattering, gray gas assumptions, and modified Planck mean absorption coefficients are applied for CO_2 and H_2O as participating medium. Ideal gas is assumed for the equation of state. The transport properties, μ, k/C_p, and ρD_j, are assumed to be proportional to $T^{0.7}$ [21]. Specific heat is a function of mixture composition and temperature [22,23]. Lewis number is assumed a constant for every species (but different for each species).

The solid phase model simulates the thermal processes of the sample and the stainless steel sample holder. The solid model considers conservation of mass and energy. A two-step pyrolysis model is considered for the sample material. The pyrolysis model was deduced by Zhao et al. and was based on thermo-gravimetric data at different heating rates [10]. Gray surface radiation is considered. The emissivity and absorptivity is set to 0.92 and reflectivity 0.08 for the stainless steel sample holder. The radiation properties of the sample are functions of the sample temperature and area density [24]. All solid properties are assumed constant (except for the sample density which decreases during pyrolysis) and are based on the literature data [20].

SIMPLER [25] algorithm was used to solve the system of the gas-phase governing equations. Convection–diffusion fluxes were discretized using power-law scheme. Discrete ordinates SN approximation (S8 with 80 ordinates) was used for the radiation transfer equation. For the solid phase model, central difference scheme was used to discretize the solid temperature gradient and fully implicit scheme was used for the unsteady terms. Strongly implicit procedure solver [26] was used for solving the resulting set of linear discretization equations for both solid and gas phases.

The model employs a nonuniform grid structure and an automatic adaptive mesh refinement scheme [18]. The program traces the flame location and allocates fine meshes (one-tenth of the

characteristic length for thermal diffusion) in the regions near the flame base and pyrolysis front while the flame spreads downstream. Here (and throughout the rest of this article), "base" and "front" refer to the most upstream and downstream points, respectively, of the burning region. The total mesh ranges from 168,720 to 452,880.

An adaptive time marching scheme is used [17,19]. For each time-step, gas-phase reaction time and solid heat-up time are evaluated. The smaller of these values is used as the reference time to determine the time-step ($dt = 1/10\ t_{ref}$).

All simulations are performed on the case high performance computing cluster at Case Western Reserve University. With parallel computing using 12 processors, simulation time ranges from 91 to 144 h for different simulated cases.

3 Numerical Results

3.1 Flow Profile for Different Sample Setups. The sample setup considered in this work (Fig. 1(b)) has an effect on the flow profile when the flow duct height is of the order of the flow boundary layer thickness. Figure 2 shows the flow profiles on the midcross section of the flow duct (the plane marked by the blue dashed line in Fig. 1(a)) for the two sample setups (with and without the side gaps, respectively) at two duct heights ($h = 7.6$ cm and $h = 2.0$ cm). For the sample setup without the side gaps (left column in Fig. 2), the boundary layer grows on the walls of the flow duct as well as on the surface of the sample holder. The effective area for the flow passage is reduced, resulting in flow speeds higher than the inlet velocity (10 cm/s) in the area between the sample holder and the ceiling of the flow duct. The maximum flow velocity increases when the height of the flow duct decreases.

For the sample setup with the side gaps (right column in Fig. 2), flow on the two sides experiences less resistance compared to the flow near the sample surface. When the flow duct height is at 2.0 cm (upper right plot in Fig. 2), the boundary layers of the duct ceiling and the sample surface meet. The flow is "locked" by the viscous boundary layer in the area between the sample and the flow duct ceiling. The side gaps ventilate most of the flow. In other words, the flowrate that the fuel sample encounters is significantly smaller than the airflow rate imposed at the duct inlet. This has a significant impact on the flame spread process and will be discussed further below.

3.2 Steady-State Concurrent-Flow Flame Spread. In most of the simulated cases, steady spread was observed. Figure 3

shows the advancement of the sample burning region for $h = 2.0$ cm. The burning region is defined by a solid pyrolysis reaction rate $>10^{-5}$ g/cm^2/s. Results of both sample setups (with and without the side gaps) show that after an initial transient period, the flame reaches a limiting length and the spread rate remains roughly constant. In this work, the steady spread rate is defined as the average spread rate of the pyrolysis front and base between 5 cm and 25 cm (see dashed–dotted linear trend lines in Fig. 3). Average pyrolysis length is also calculated over the same period of time.

For the sample setup with the side gaps, the flame is shorter and spreads slower compared to the setup without the side gaps. This is because the flame encounters a smaller flow with side gaps present, as explained above.

The steady-state pyrolysis lengths and spread rates are plotted against flow duct height in Fig. 4. Also shown on the plot is the data from the previous microgravity experiments with the same flow conditions. Note that the pyrolysis lengths obtained in the simulations and the experiments are subject to the criteria used to define the flame or pyrolysis regions. In the experiments, the flame length is determined through flame image analysis and may depend on the camera settings (e.g., exposure and gain). Detailed comparisons of the transient flame spread process between the simulations and experiments can be found in a previous paper [10].

For both sample setups, the pyrolysis length and spread rate first increase and then decrease when the flow duct height is reduced, consistent with previous work [14,15]. Among the simulated cases, the optimal flow duct height for the flame spread occurs at 3.0–4.0 cm. When the flow duct height is below a critical value (~0.5–0.8 cm), the flame fails to spread to the end of the sample.

3.3 Effect of the Height of the Flow Duct on Flame Spread. To understand this nonmonotonic trend, solid and gas profiles are examined in detail. Figure 5 shows the oxygen profiles on the center symmetry plane. Figures 6 and 7 compares the heat flux distributions on the sample surface and duct ceiling at the steady-states. For these profiles, the two sample setups have similar results and hence only results for the sample setup with side gaps are shown here. Figure 5 shows that when the duct height is sufficiently large (e.g., $h = 4.0$ cm), oxygen is transported (via convection and diffusion) to the downstream end of the duct. As the duct height is reduced, the mass flowrate of the air (and the oxygen) is expected
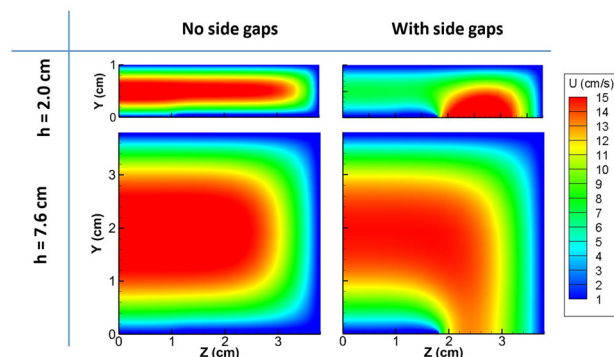

Fig. 2 Flow velocity profile on the midcross section of the flow duct (20 cm from the upstream leading edge of the sample holder, as marked by the blue dashed line in Fig. 1(a)). Flow velocity at the flow duct inlet: 10 cm/s. Results are from pure flow simulation without combustion. The vertical axis, Y (cm), is the distance from the sample surface and the horizontal axis, Z (cm), is the distance from the center-symmetric plane of the flow duct.
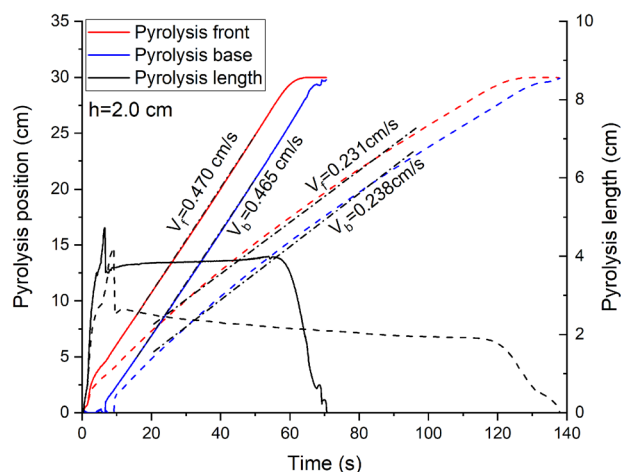

Fig. 3 Location of downstream pyrolysis front, upstream pyrolysis base, and pyrolysis length versus time for $h = 2.0$ cm. Dash lines are for sample setup with side gaps. Solid thick lines are for sample setup without side gaps. Black dashed–dotted lines are linear fitting trend lines of the pyrolysis positions.
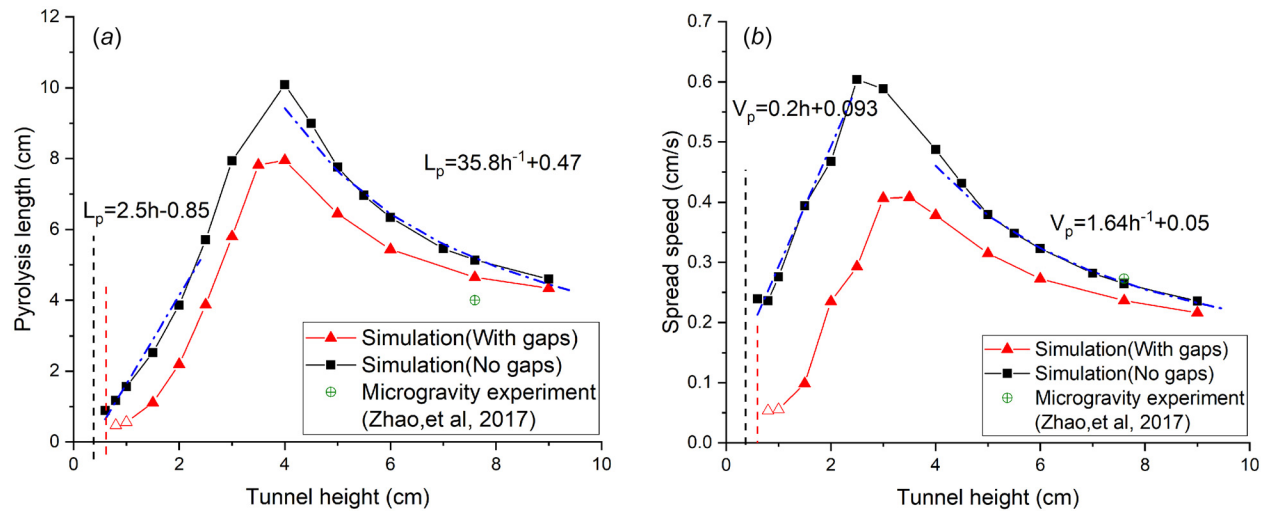
Fig. 4 (a) Pyrolysis lengths and (b) flame spread rates versus flow duct heights. The dash lines denote the quench limits. Hollow symbols denote partial propagation.

to decrease since a constant air velocity is imposed at the duct inlet in all cases. Figure 5 also shows that for $h = 2.0$ cm, the flame extends to the duct ceiling and consumes all the oxygen. This implies that the oxygen supply becomes a limiting factor for the combustion in the downstream region. The reduced oxygen supply to the flame and to the downstream region may contribute to the shorter pyrolysis length and the smaller spread rate for $h = 2.0$ cm compared to $h = 4.0$ cm.

Figure 6 show the heat flux distributions on the sample surface (Fig. 6(a)) and the duct ceiling (Fig. 6(b)) for $h = 2.0$ cm and 7.6 cm. Figure 7 further compares the heat fluxes along the centerline of the sample for three different duct heights. The heat fluxes along the sample centerline for $h = 4.0$ cm and $h = 7.6$ cm are of similar magnitudes. Conductive heat to the ceiling is negligible as the flame is far away from the ceiling. The heat loss to the ceiling is mainly due to flame radiation (hence the curves coincide with the net heat flux onto the duct ceiling for $h = 4.0$ and 7.6 cm in Fig. 7). At $h = 2.0$ cm, the flame is in close proximity to the duct ceiling (see Fig. 5). Both conduction and radiation account for the heat losses from the flame to the duct ceiling. Note that the conductive heat loss to the ceiling is comparable to the conductive heat feedback to the sample surface. Also note that at $h = 2.0$ cm, the radiation heat loss to the ceiling is approximately twice of that at $h = 4.0$ cm and 7.6 cm.

For heat fluxes on the sample surface, Figs. 6(b) and 7 show that the conductive heat flux from the flame to the sample surface increases as the height of the flow duct decreases. This is
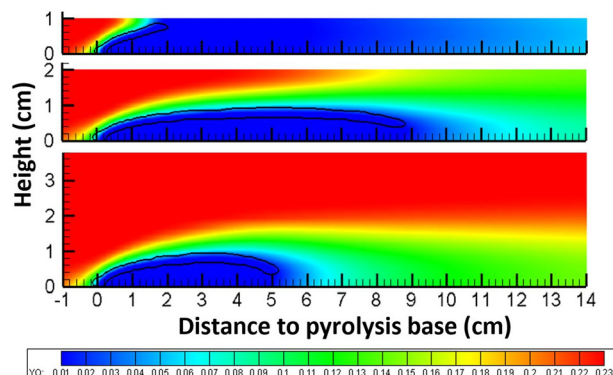
reasonable as the confinement imposed by the duct ceiling forces the flame to stay close to the sample surface, enhancing the conductive and net heat fluxes near the upstream flame base region. As a consequence, higher local burning rate (or fuel mass flux on the sample) at the upstream flame base region is expected for a smaller duct height, despite the fact that the pyrolysis length might be smaller due to the oxygen limitation in the downstream region.

The flow velocity profiles at different flow duct heights are also compared. Figures 8 shows profiles at the center symmetry plane for $h = 2.0$ cm, 4.0 cm, and 7.6 cm. For $h = 4.0$ cm and 7.6 cm, flow profiles on the center plane using the two different sample setups are similar (hence only one result is shown). It is evident that in these cases (large duct heights), the flow accelerates due to the thermal expansion during the combustion process. This effect becomes more and more significant when the duct height decreases. Compared to $h = 7.6$ cm, the flow for $h = 4.0$ cm is stronger, and as a result, the flame is longer.

For small duct heights (e.g., $h = 2.0$ cm in Fig. 8), simulations with sample setup with and without side gaps show different results. For sample setups without the side gaps, the flow accelerates due to thermal expansion as discussed above. However, when side gaps are present, flow is diverted to the side gaps. The flow speed on the center symmetry plane is low even after thermal expansion. This effect, in addition to the reduced oxygen supply and the increased heat loss to the ceiling, contributes to the decreased spread rate and pyrolysis length when duct height decreases. Note that both the quenching height and the optimal duct height for flame spread are slightly higher for sample setups with side gaps compared to those without gaps.

In summary, when the heights of the flow duct are sufficiently large (e.g., $h > 4.0$ cm), flow confinement affects the flame mainly through flow acceleration during thermal expansion. For similar volumetric expansion, flow acceleration is expected to be inversely related to the duct cross-sectional area (or the duct height in this study). This is consistent with the observation in Fig. 4: the flame spread rate shows inverse relationship to the duct height ($V_f \sim 1/h$) at large duct heights.

When the heights are near the quenching limit (e.g., $h = 2.0$ cm), the limitation of the oxygen supply to the combustion zone plays an important role. The flame spread rate and the pyrolysis length are expected to grow with the oxygen volumetric supply rate (or the duct height in this study). Figure 4 shows that the flame spread rate is approximately linear to the duct height ($V_f \sim h$) at small duct heights.

Fig. 5 Mass fraction of oxygen (background contours) and flame shape (thick lines) on the center symmetry plane. From to top to bottom: $h = 2.0$ cm, $h = 4.0$ cm, and $h = 7.6$ cm. Flame shape is defined as the gas phase reaction at 10^{-4} g/cm^3/s.

3.5 Near Limit Oscillation. As mentioned above, there exists a quenching duct height below which no flame spread is
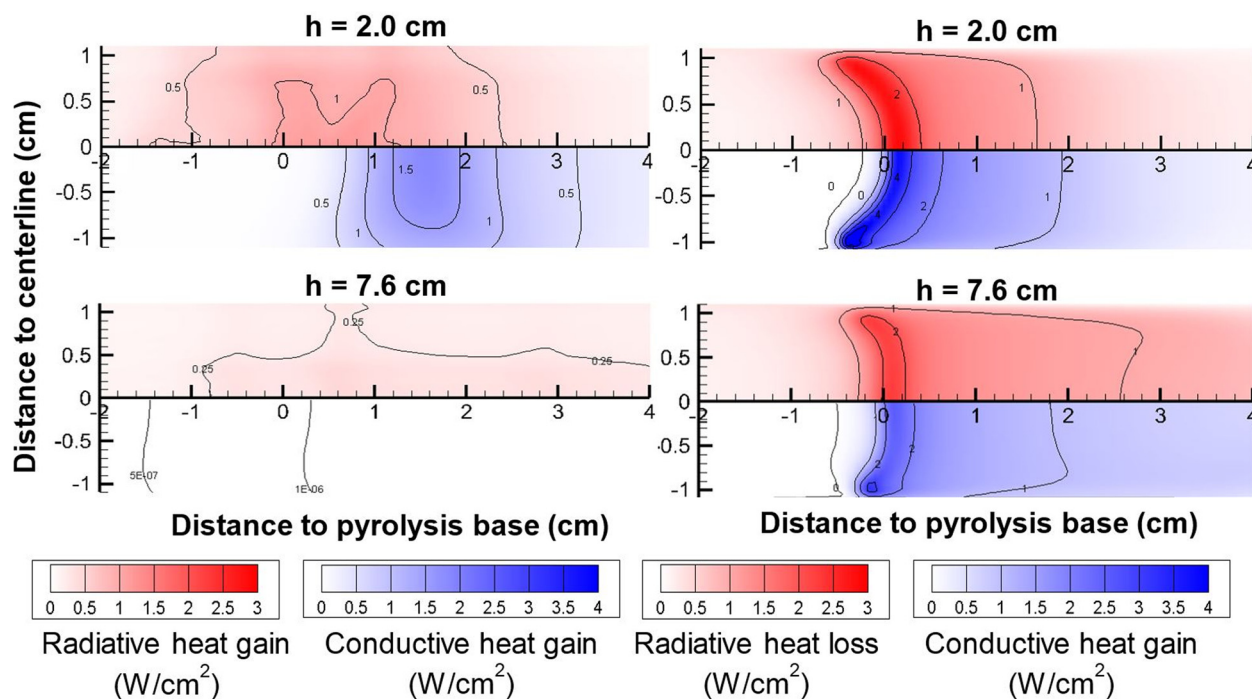
Fig. 6 Conductive and radiative heat flux distributions on (*a*) the duct ceiling and (*b*) the sample surface for $h = 2.0$ cm and $h = 7.6$ cm
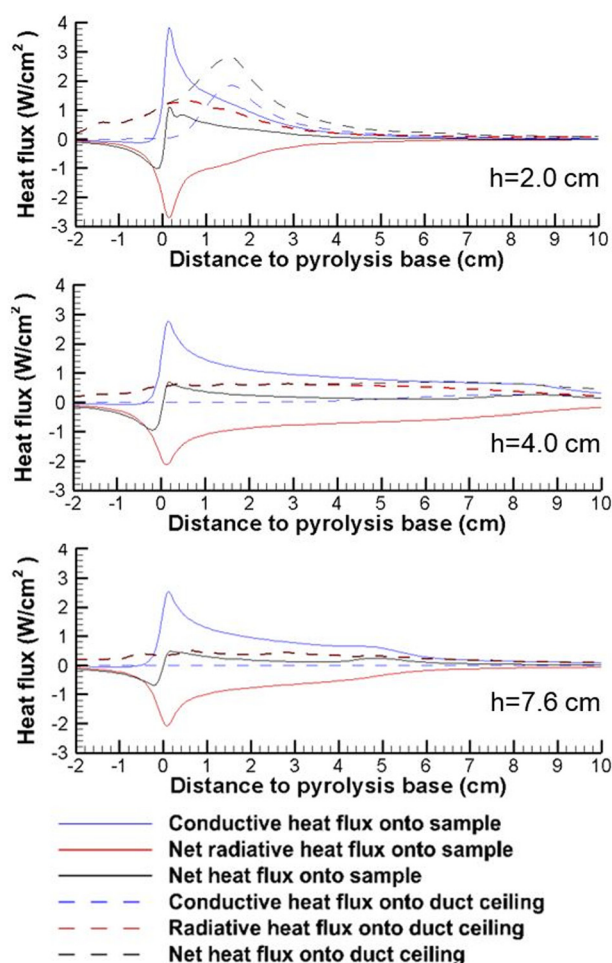

Fig. 7 Heat flux distributions along the sample centerline. From top to bottom: $h = 2.0$ cm, $h = 4.0$ cm, and 7.6 cm.

observed. Near this limit, for the sample setup with side gaps, flow near the sample surface was very low (~ 3–5 cm/s) and the pyrolysis length was observed to oscillate (Fig. 9). Similar oscillations in flame length was reported in previous works for candle flames [27], edge flames [28], pool fires [29], and opposed-flow diffusion flames [30], and has been attributed to thermodiffusive instability. The thermodiffusive instability of solid combustion usually arises near the flame quenching limit with nonunity effective Lewis number. The imbalance of heat loss and oxygen supply to flames leads to flame shape oscillations. The simulation results in this work further show that not only does pyrolysis length oscillate, but the maximum gas temperature and its location relative to the upstream pyrolysis base also oscillates with the same frequencies (Fig. 10).
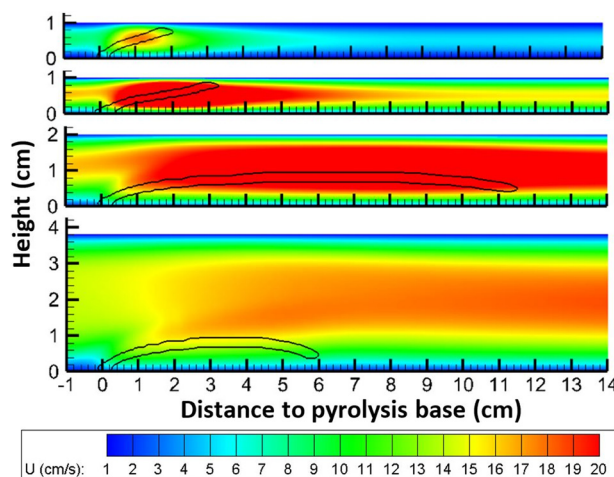

Fig. 8 Streamwise flow velocity (background contours) and flame shape (thick lines) on the center symmetry plane. From top to bottom: $h = 2.0$ cm (with side gaps), $h = 2.0$ cm (without side gaps), $h = 4.0$ cm, $h = 7.6$ cm. Flame shape is defined as the gas phase reaction at 10^{-4} g/cm^3/s.
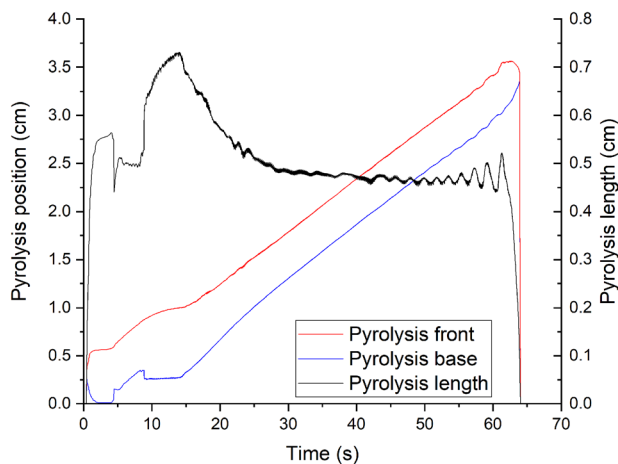
Fig. 9 Near quenching oscillation: location of pyrolysis front, pyrolysis base, and pyrolysis length on the center symmetry plane ($h = 0.8$ cm for sample setup with side gaps)
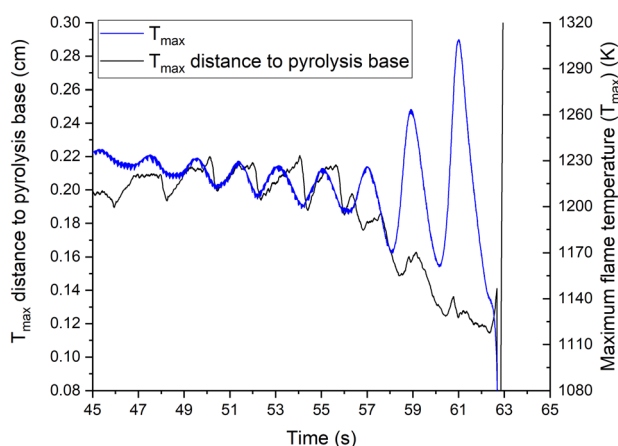

Fig. 10 Near quenching oscillation: maximum gas temperature and its position relative to the upstream pyrolysis base ($h = 0.8$ cm with sample setup with side gaps

The flame and solid profiles in one cycle (~ 2 s) of the flame oscillations are examined in Fig. 11. The solid mass loss rate (see black lines in Fig. 11 bottom plots) indicates that the flame splits and merges in the lateral (cross stream) direction. In the first half of the cycle, two flamelets near the sample sides grow laterally and merge at the center. In the second half of the cycle, the flame splits laterally and forms two flamelets. Then, the next period starts.

The laterally splitting flames (or the flamelets) were similar to the fingering flames observed near quenching conditions in previous work [31,32]. In a study of Wang et al. [32], flame bifurcated and formed two flamelets in a low-speed concurrent flow in a narrow simulated-zero-gravity flow channel. Note that the conditions (1.1 cm channel height, 3 cm/s imposed flow) and the flame spread rate (0.047 cm/s) in their work are similar to those presented in Fig. 11. In our work, as mentioned above, although 10 cm/s flow was imposed in the flow duct inlet, the local flow velocity the sample encountered was significantly lower (3–5 cm/s) due to the presence of the side gaps.

Similarly, Olson et al. observed finger-shaped burn patterns for opposed flow flame spread [31]. They further proposed that such flame bifurcations increase the surface to volume ratio of the flame, which in turn enhances the oxygen transport to the flames. They also proposed that the formation of flamelets helps focus the heat release in a small volume, providing sufficient heat flux to the unburnt fuel beneath. Both of these help the flame to survive on the margin of flammability.

In this work, the characteristic thermal and oxygen diffusion times across the sample width are $t_{thermal} = W_s^2/\alpha^* = 2.3$ s and $t_{oxygen} = W_s^2/D^* = 2.5$ s, respectively, (W_s is the sample width, α^* and D^* are the thermal and species diffusivity at the reference temperature 1250 K). These time scales are of the same magnitude of the period of the flame oscillation (~ 2 s). This further suggests that the thermodiffusive instability accounts for the flame oscillations before the flame quenches.

4 Conclusion

A three-dimensional transient CFD code was used to simulate concurrent-flow flame spread over thin solid materials in a low-speed flow duct in microgravity. The height of the flow duct is
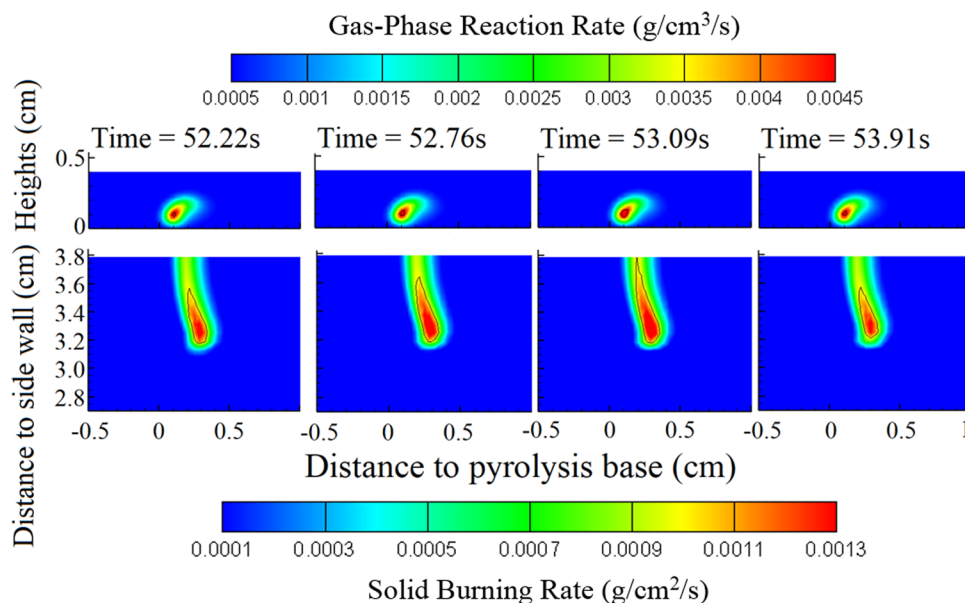
Fig. 11 One cycle of the flame oscillation. Top: reaction rate contour on the center symmetry plane. The solid line denotes reaction rate at 0.0045 g/cm³/s. Bottom: mass loss rate on solid surface. The solid line denotes mass loss rate at 0.001 g/cm²/s.

varied to study the effect of confinement and the flame-wall aero-dynamics/thermal interactions. The main findings are as follows.

(1) In most simulated cases, the flame reaches a steady spreading state before the sample is consumed. The flame spread rate and the pyrolysis length at steady-state first increase and then decrease when the flow duct height decreases.

(2) The flow confinement imposed by the duct has multiple effects on the flame spreading process. On one hand, it accelerates the flow when the flow experiences thermal expansion during combustion. The confinement also forces the flame to stay close to the sample surface, enhancing the net heat flux and local solid burning rate near the upstream flame base. These effects intensify the flame. On the other hand, it limits the oxygen supply to the flame in the downstream region. The flame also loses heat to the duct walls through conduction and radiation, reducing the strength of the flame. These competing effects results in the above-mentioned non-monotonic trend of the flame spread rate and pyrolysis length at different duct heights.

(3) When the duct height is on the order of the thickness of the flow viscous boundary layer, the setup of the sample plays a significant role on the experiment. In this study, a flat thin sample is placed in the center of the flow duct and it (or its holder) does not span across the width of the duct, leaving gaps on the two sides. Flow is diverted to the side gaps and the actual flow speed in the sample region is significantly lower than the flow imposed at the duct inlet. This reduces the flammability of the sample.

(4) When the height of the duct is below a critical quenching height, no flame spread is observed. Near this limit, oscillation of the pyrolysis length is observed. The flame splits and merges periodically in the lateral direction before the flame dies. This phenomenon is suspected to be due to thermodiffusive instability and will be investigated further in future work.

Acknowledgment

Funding Data

References

[1] Evarts, B., 2019, *Fire Loss in the United States During 2018*, National Fire Protection Association, Quincy, MA.

[2] Lattimer, B. Y., and Usman, S., 2003, "Thermal Characteristics of Fires in a Noncombustible Corner," Fire Saf. J., **38**(8), pp. 709–745.

[3] Poreh, M., and Gordon, G., 2000, "A Study of Wall and Corner Fire Plumes," Fire Saf. J., **34**(1), pp. 81–98.

[4] Jamison, K. L. T., and Boardman, D. A., 2016, "A New Fire Performance Test for Cavity Wall Insulation," MATEC Web of Conferences, **46**, p. 02004.

[5] Hu, L. H., Peng, W., and Huo, R., 2008, "Critical Wind Velocity for Arresting Upwind Gas and Smoke Dispersion Induced by Near-Wall Fire in a Road Tunnel," J. Hazard. Mater., **150**(1), pp. 68–75.

[6] Tian, X., Zhong, M., Shi, C., Zhang, P., and Liu, C., 2017, "Full-Scale Tunnel Fire Experimental Study of Fire-Induced Smoke Temperature Profiles With Methanol-Gasoline Blends," Appl. Therm. Eng., **116**, pp. 233–243.

[7] Ferkul, P. V., and T'ien, J. S., 1994, "A Model of Low-Speed Concurrent Flow Flame Spread Over a Thin Fuel," Combust. Sci. Technol., **99**(4–6), pp. 345–370.

[8] Tseng, Y.-T., and T'ien, J. S., 2010, "Limiting Length, Steady Spread, and Non-growing Flames in Concurrent Flow Over Solids," ASME J. Heat Transfer, **132**(9), p. 091201.

[9] Olson, S. L., and Ferkul, P. V., 2015, "Microgravity Flammability of PMMA Rods in Concurrent Flow," Nineth U.S. National Combustion Meeting, Cincinnati, OH, May 17–20.

[10] Zhao, X., Liao, Y.-T. T., Johnston, M. C., T'ien, J. S., Ferkul, P. V., and Olson, S. L., 2017, "Concurrent Flame Growth, Spread, and Quenching Over Composite Fabric Samples in Low Speed Purly Forced Flow in Microgravity," Proc. Combust. Inst., **36**(2), pp. 2971–2978.

[11] Olson, S. L., Ferkul, P. V., Bhattacharjee, S., Miller, F. J., Fernandez-Pello, C., Link, S., T'ien, J. S., and Wichman, I., 2015, "Results From on-Board CSA-CP and CDM Sensor Readings During the Burning and Suppression of Solids—II (BASS-II) Experiment in the Microgravity Science Glovebox (MSG)," 45th International Conference on Environmental Systems, Bellevue, WA, July 12–16, Paper No. ICES-2018-196.

[12] Li, C., Liao, Y.-T. T., T'ien, J. S., Urban, D. L., Ferkul, P., Olson, S., Ruff, G. A., and Easton, J., 2018, "Transient Flame Growth and Spread Processes Over a Large Solid Fabric in Concurrent Low-Speed Flows in Microgravity—Model Versus Experiment," Proc. Combust. Inst., **37**(3), pp. 4163–4171.

[13] Urban, D. L., Ferkul, P., Olson, S., Ruff, G. A., Easton, J., T'ien, J. S., Liao, Y.-T. T., Li, C., Fernandez-Pello, C., Torero, J. L., Legros, G., Eigenbrod, C., Smirnov, N., Fujita, O., Rouvreau, S., Toth, B., and Jomaas, G., 2019, "Flame Spread: Effects of Microgravity and Scale," Combust. Flame, **199**, pp. 168–182.

[14] Shih, H.-Y., and T'ien, J. S., 1997, "Modeling Wall Influence on Solid-Fuel Flame Spread in a Flow Tunnel," AIAA Paper No. 97-0236.

[15] Shih, H.-Y., 2009, "Flame Spread and Interactions in an Array of Thin Solids in Low-Speed Concurrent Flows," Combust. Theory Modell., **13**(3), pp. 443–459.

[16] Malhotra, V., Kumar, C., and Kumar, A., 2013, "Opposed Flow Flame Spread Over an Array of Thin Solid Fuel Sheets in a Microgravity Environment," Combust. Theory Modell., **17**(5), pp. 835–857.

[17] Liao, Y.-T. T., and T'ien, J. S., 2013, "A Numerical Simulation of Transient Ignition and Ignition Limit of a Composite Solid by a Localised Radiant Source," Combust. Theory Modell., **17**(6), pp. 1096–1124.

[18] Zhao, X., and T'ien, J. S., 2015, "A Three-Dimensional Transient Model for Flame Growth and Extinction in Concurrent Flows," Combust. Flame, **162**(5), pp. 1829–1839.

[19] Tseng, Y.-T., 2011, "Three-Dimensional Model of Solid Ignition and Ignition Limit by a Non-Uniformly Distributed Radiant Heat Source," Ph.D. dissertation, Case Western Reserve University, Cleveland, OH.

[20] Li, C., and Liao, Y.-T. T., 2018, "Numerical Investigation of Flame Splitting Phenomenon in Upward Flame Spread Over Solids With a Two-Stage Pyrolysis Model," Combust. Sci. Technol., **190**(12), pp. 2082–2096.

[21] Smoke, M. D., and Giovangigli, V., 1991, "Formulation of the Premixed and Nonpremixed Test Problems," Reduced Kinetic Mechanisms and Asymptotic Approximations for Methane-Air Flames, Springer, Berlin, pp. 1–28.

[22] Lefebvre, A. W., 1983, Gas Turbine Combustion, McGraw-Hill, New York.

[23] Zucrow, M. J., and Hoffman, J. D., 1976, Gas Dynamics, Wiley, New York.

[24] Richard, P., 2015, "Radiative Characteristics of a Thin Solid Fuel at Discrete Levels of Pyrolysis: Angular, Spectral, and Thermal Dependencies," Ph.D. dissertation, Case Western Reserve University, Cleveland, OH.

[25] Patankar, S. V., 1980, *Numerical Heat Transfer and Fluid Flow*, Hemisphere, New York.

[26] Perić, H. L. a. M., 1994, "Vectorized Strongly Implicit Solving Procedure for a Seven-Diagonal Coefficient Matrix," Int. J. Numer. Meth. Heat Fluid Flow, **4**(2), pp. 159–172.

[27] Dietrich, D. L., Ross, H. D., Shu, Y., Chang, P., and T'ien, J. S., 2000, "Candle Flames in Non-Buoyant Atmospheres," Combust. Sci. Technol., **156**(1), pp. 1–24.

[28] Buckmaster, J., and Zhang, Y., 1999, "Oscillating Edge-Flames," Combust. Theory Modell., **3**(3), pp. 547–565.

[29] Schiller, D. N., Ross, H. D., and Sirignano, W. A., 1996, "Computational Analysis of Flame Spread Across Alcohol Pools," Combust. Sci. Technol., **118**(4–6), pp. 203–255.

[30] Kumar, K. M. N., and Kumar, A., 2017, "The Dynamics of Near Limit Self-Propagating Flame Over Thin Solid Fuels in Microgravity," Proc. Combust. Inst., **36**(2), pp. 3081–3087.

[31] Olson, S. L., Miller, F. J., Jahangirian, S., and Wichman, I. S., 2009, "Flame Spread Over Thin Fuels in Actual and Simulated Microgravity Conditions," Combust. Flame, **156**(6), pp. 1214–1226.

[32] Wang, S., Wang, S., Zhu, K., Xiao, Y., and Lu, Z., 2016, "Near Quenching Limit Instabilities of Concurrent Flame Spread Over Thin Solid Fuel," Combust. Sci. Technol., **188**(3), pp. 451–471.